

The Vertical Structure and Kinematics of Grand Design Spirals

Victor P. Debattista^{1*}

¹ *Jeremiah Horrocks Institute, University of Central Lancashire, Preston PR1 2HE, UK*

Draft version on 27 May 2014

ABSTRACT

We use an N -body simulation to study the 3-D density distribution of spirals, and the resulting stellar vertical velocities. Relative to the disc’s rotation, the phase of the spiral’s peak density away from the mid-plane trails that at the mid-plane. In addition, at fixed radius the density distribution is azimuthally skewed, having a shallower slope on the trailing side inside corotation and switching to shallower on the leading side beyond corotation. The spirals induce non-zero average vertical velocities, $\langle V_z \rangle$, as large as $\langle V_z \rangle \sim 10 - 20 \text{ km s}^{-1}$, consistent with recent observations in the Milky Way. The vertical motions are compressive (towards the mid-plane) as stars enter the spiral, and expanding (away from the mid-plane) as they leave it. Since stars enter the spiral on the leading side outside corotation and on the trailing side within corotation, the relative phase of the expanding and compressive motions switches sides at corotation. Moreover, because stars always enter the spiral on the shallow density gradient side and exit on the steeper side, the expanding motions are larger than the compressing motions.

Key words: Galaxy: disc – Galaxy: kinematics and dynamics – Galaxy: structure – galaxies: interactions – galaxies: kinematics and dynamics – galaxies: spiral

1 INTRODUCTION

Spiral structure is one of the defining characteristics of disc galaxies. As a result, significant effort has been expended on understanding the generation and dynamics of spirals. The standard interpretation views spirals as density waves in the stellar distribution, but the cause of these waves, when not triggered by bars or external perturbations, remains uncertain. Models proposed include the swing amplification of noise (Goldreich & Lynden-Bell 1965; Julian & Toomre 1966), groove modes (Sellwood & Lin 1989; Sellwood & Kahn 1991; Sellwood 2012) or other modes (Lin & Shu 1964), possibly recurrent (Sellwood & Carlberg 2014). Gas plays an important role in the life cycle of spirals, both by cooling the disc, allowing further generations of spirals (Sellwood & Carlberg 1984), and by providing granularity in the disc potential helpful in exciting spirals (D’Onghia et al. 2013). The realization that spirals can drive substantial radial mixing without heating (Sellwood & Binney 2002; Roškar et al. 2008; Schönrich & Binney 2009) has led to a significant resurgence of interest in the problem of spiral structure formation and evolution.

Widrow et al. (2012) reported an asymmetry in the density distribution across the Milky Way’s mid-plane from SEGUE data, which was explored further by Yanny & Gardner (2013). Additionally, large-scale, coherent vertical motions have been found in the Milky Way’s disc in SEGUE (Widrow et al. 2012), RAVE (Williams et al. 2013) and LAMOST (Carlin et al. 2013) data. Prior to these studies, Bochanski et al. (2011) had found a variation by spectral type in the vertical velocity of a sample of M-dwarfs, although they could not distinguish these from the effect of distance variations arising from differences in absolute magnitude due to metallicity differences. Widrow et al. (2012) and Gómez et al. (2013) proposed that these asymmetries result from bending caused by an interaction with substructure. However, a puzzling feature of the vertical velocities is that the dominant motion corresponds to a breathing mode of the disc, *i.e.* stars on either side of the mid-plane are coherently moving either away from or towards the mid-plane. A bend in the disc caused by a perturber would instead lead to motions that have the same direction on both sides of the mid-plane. Schönrich (2012) cautioned that these motions may be due to residual errors in the survey pipeline. Nevertheless, in the anti-centre direction, Carlin et al. (2013) now find stellar motions towards the mid-plane extending to 2 kpc from the Sun.

* E-mail: vpdebattista@gmail.com

These observations raise the question of whether internal causes are possible and impel us to study the vertical structure and kinematics of spirals. To a large extent spirals have been studied in the two-dimensional approximation under the simplifying assumption that the motions of stars in the planar direction are decoupled from the vertical motion. Recently, Faure et al. (2014) presented 3D test particle orbits in a spiral potential, showing that spirals induce vertical motions consistent with the Milky Way observations. In this Letter, we study the 3D density distribution of spirals and the effect this has on the vertical motions using self-consistent N -body simulations.

2 MODEL SETUP

We use simulation II of Meidt et al. (2008) which was designed to have a single grand design spiral with a well-defined pattern speed. This consists of a compact bulge and an exponential disc, immersed in a spherical halo potential. The disc has an exponential surface density profile with mass M_d and scalelength R_d ; it is truncated at $5R_d$. The vertical profile is Gaussian with a scaleheight $z_d = 0.1R_d$. We set the Q -parameter of the disc (Toomre 1981) to $Q = 1.2$ using the epicyclic approximation. In order to slow the formation of a bar till well after a spiral has formed, we include a massive compact bulge. The bulge was generated from an isotropic distribution function (DF) of polytrope form $F(E) \propto (-E)^n$, with $n = \frac{7}{2}$, using the method of Prendergast & Toomer (1970) as described in Debattista & Sellwood (2000). The DF was integrated iteratively until convergence in the global potential. The bulge has a mass $M_b = \frac{1}{3}M_d$ and is truncated at $r_t = 1.51R_d$. The dark matter halo is represented by a rigid potential of the form $\Phi_h = \frac{1}{2}V_h^2 \ln(r^2 + r_h^2)$; we set $V_h = 0.65$ and $r_h = 5R_d$.

The disc is initially populated by 3 million particles. We set up particles in groups of four: the first particle in each quartet has (x, y, z, v_x, v_y, v_z) while the rest have $(-x, -y, z, -v_x, -v_y, v_z)$, $(x, y, -z, v_x, v_y, -v_z)$ and $(-x, -y, -z, -v_x, -v_y, -v_z)$. Besides ensuring that the centre of the system does not move because of noise, this quiet start (Sellwood 1983) has the desirable property that the disc is highly symmetric about the mid-plane, ensuring that no small-scale bends are present. The main disadvantage is that it reduces the number of independent particles, so that statistically it is equivalent to only $\sim 7.5 \times 10^5$ particles. In order to produce a strong spiral, we seed the disc with a groove mode (Sellwood & Lin 1989; Sellwood & Kahn 1991) by removing all particles in the specific angular momentum range $1.6 < l_z < 1.8$ in units where $R_d = M_d = G = 1$. This results in the removal of 5.6% of the disc's mass.

The system was evolved with the cylindrical polar grid code of Sellwood & Valluri (1997). This solves for the potential by expansion in a Fourier series in the ϕ direction, via a fast Fourier transform in the vertical direction, and by convolution with the Green function in the radial direction. We use Fourier terms up to $m = 8$ in the potential solver (excluding $m = 1$ in order that the system remains centred at the origin). The grid has $n_R \times n_\phi \times n_z = 60 \times 64 \times 243$ grid cells. The vertical spacing of the grid cells is $0.125z_d$, and the radial spacing is logarithmic, reaching to $10R_d$. Our

timestep is $\delta t = 0.001$. We set the softening length of all particles to $\epsilon = 0.017R_d$.

We adopt a scaling to real units for facilitating comparison with the Milky Way which has $R_d = 2.5$ kpc and $V_h = 228 \text{ km s}^{-1}$, which produces a mean streaming velocity, $\langle V_\phi \rangle$, at 8 kpc of $\sim 220 \text{ km s}^{-1}$. This scaling corresponds to a unit of time equal to 7.1 Myr. Meidt et al. (2008) showed that the spiral that forms has a corotation (CR) radius at ~ 5 kpc in our rescaled units.

3 RESULTS

Fig. 1 shows the projected surface density after a strong $m = 2$ grand design spiral forms. The spiral has maximum surface density contrast $\delta\Sigma/\langle\Sigma\rangle \simeq 2.5$, or peak Fourier $m = 2$ amplitude $A_{2,peak} \simeq 0.65$ (see fig. 13 of Meidt et al. (2008)), making this a very strong, grand design spiral (Rix & Zaritsky 1995). Fig. 1 overplots a logarithmic spiral, $\phi \propto 2 \cot \gamma \ln R$, with pitch angle $\gamma = 40^\circ$ which matches the peak surface density well. In comparison, the Milky Way's spirals have a pitch angle $\gamma \sim 10^\circ$ (e.g. Siebert et al. 2012).

3.1 Density distribution

Fig. 2 maps the density in the (ϕ, z) -plane for 1-kpc-wide annuli. At each radius, the peak density in the mid-plane is ahead (relative to the direction of rotation) of the peak density at higher $|z|$, resulting in wedge-shaped isodensity contours in cross-section. Since each annulus projects through a range of radii, some of this offset may be caused by the radial superposition of a winding spiral. Therefore Fig. 1 plots the phase of the $m = 2$ density moment, ϕ_2 , for slices in $|z|$ of width $\delta z = z_d = 250$ pc. The bottom panel shows these phases as a function of radius, while the top panel plots these phases over the surface density distribution. Relative to the sense of rotation, the phase lag from the mid-plane increases with height, from $\gtrsim 5^\circ$ at $2 - 3z_d$ to $\gtrsim 20^\circ$ by $3 - 4z_d$.

Fig. 2 also shows that the density distribution at fixed R and z is asymmetric in ϕ relative to the peak density. Fig. 3 plots the density distribution as a function of ϕ for two radii, one inside CR ($R = 3.9$ kpc) and one outside ($R = 6.5$ kpc), showing explicitly that the density distribution is skewed. The skewness changes sense across CR: inside, the shallower side is behind the peak while outside it is ahead of the peak. Thus, stars always enter the spiral on the shallower density slope side and exit it on the steeper side, regardless of which side of CR they are on. This asymmetry arises because as the density wave propagates through the disc, stars on low eccentricity orbits are better able to maintain phase with it, whereas stars on higher eccentricity orbits trail the spiral.

3.2 Vertical Kinematics

We now turn to the trace of the spiral in the vertical velocities. Fig. 4 presents the mean vertical velocity, $\langle V_z \rangle$ in the annulus $4 \leq R/\text{kpc} \leq 5$. Generally, $\langle V_z \rangle$ is quite small, but non-zero. Fig. 4 also shows that the peak $|\langle V_z \rangle|$ increases with height. The data of Widrow et al. (2012) and Carlin et al. (2013) also show a trend of increasing $\langle V_z \rangle$ with $|z|$.

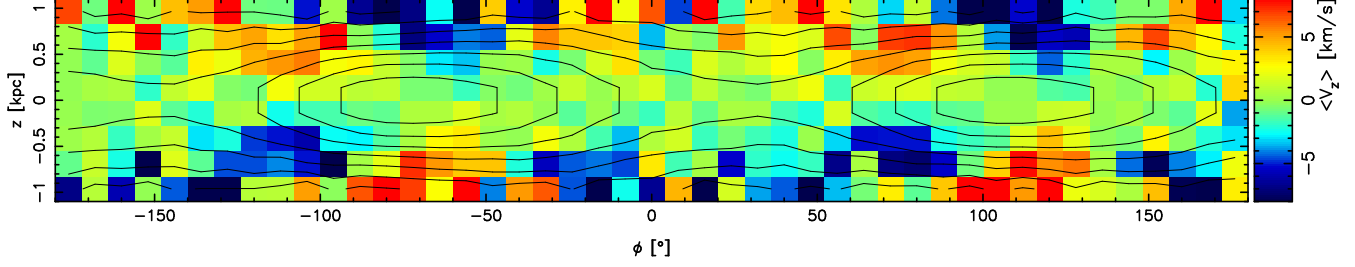


Figure 4. Average vertical velocity, $\langle V_z \rangle$, in the annulus $4 \leq R/\text{kpc} \leq 5$, just inside CR. The sense of rotation is towards decreasing ϕ . As in Fig. 2, the volume density is indicated by the contours, which are separated by a factor of 2.3.

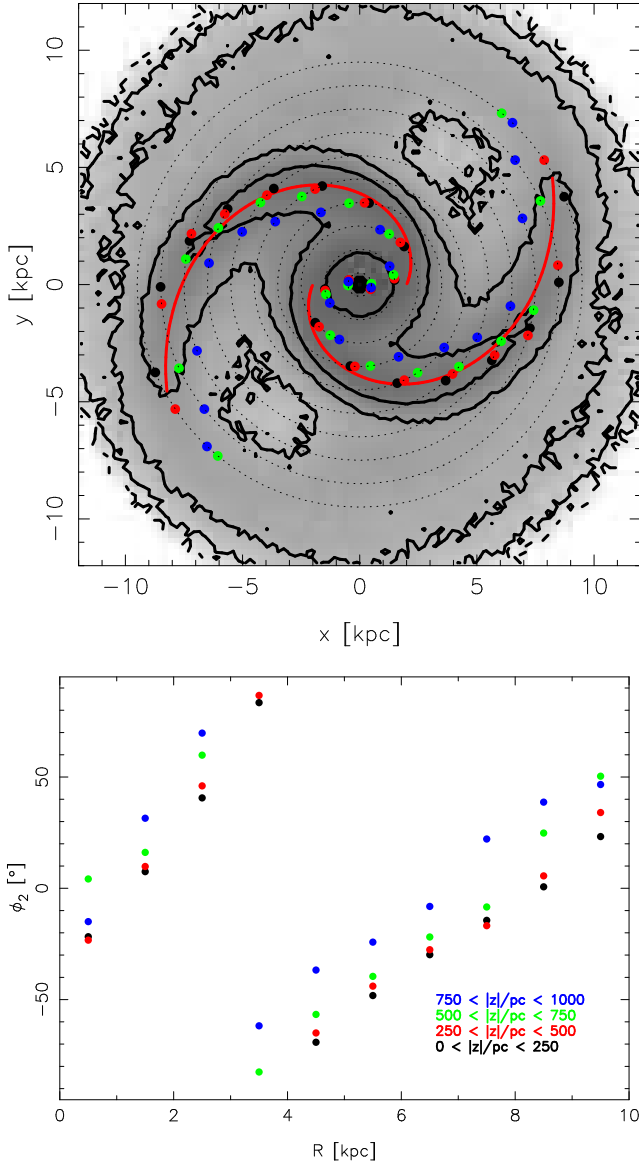


Figure 1. Top: surface density of the model at 3.8 Gyr. The red lines show an $m = 2$ logarithmic spiral of pitch angle $\gamma = 40^\circ$. The dotted circles represent the constant radius from 0.5 to 9.5 kpc, in 1 kpc intervals. The filled circles indicate ϕ_2 at that radius with $|z|$ colour-coded as in the bottom panel. Bottom: phase of the $m = 2$ perturbation for four slices in $|z|$ each of width $\delta z = z_d = 250$ pc. Different slices are colour-coded as indicated.

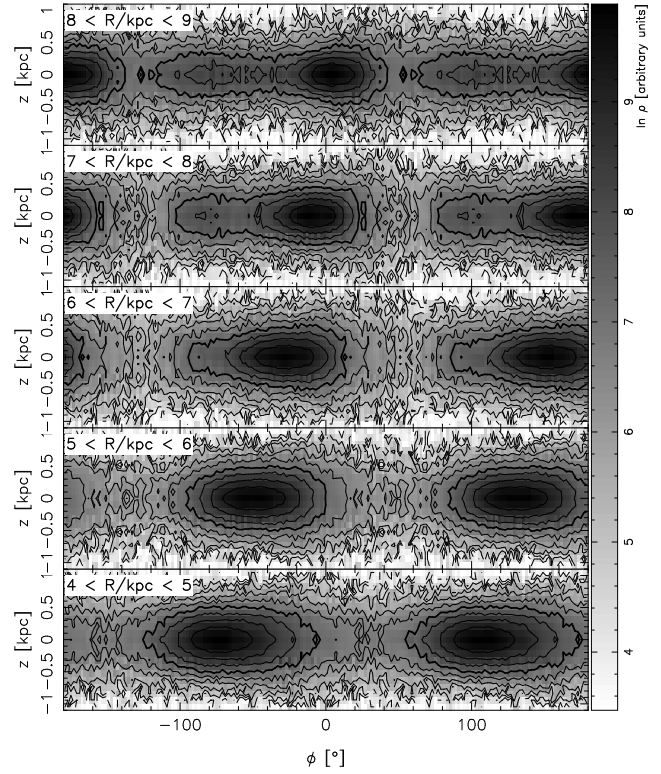


Figure 2. The stellar volume density in annuli as indicated in each panel. The sense of rotation is towards decreasing ϕ . Contours are separated by a factor of 1.9. The bold contour represents a common value.

Fig. 5 plots the vertical velocity asymmetry, which we define as:

$$\Delta V_z = \frac{\sum_{\text{bins}, z>0} \langle V_z \rangle - \sum_{\text{bins}, z<0} \langle V_z \rangle}{N_{\text{bins}}/2}. \quad (1)$$

Note that Equation 1 first computes the average V_z in each vertical bin before calculating the difference across the mid-plane; as a result, ΔV_z is not dominated by the high-density bins nearest $z = 0$. Wherever ΔV_z is negative the motions are compressive, whereas they are expanding when it is positive. We use six bins in z , in the range $-3z_d \leq z \leq 3z_d$. Non-zero vertical motions can clearly be seen in Fig. 5. The relative sense of compression versus expansion changes across the CR radius; inside this radius vertical motions are compressive behind the spiral peak and expanding ahead of it. Outside CR the sense shifts and compression (expansion) happens ahead (behind) the spiral peak.

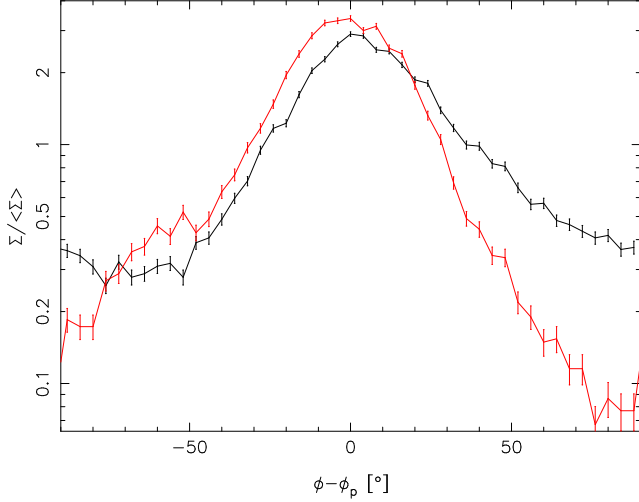


Figure 3. The density distribution as a function of phase relative to the phase of the peak density. The black line shows the density distribution at 3.9 kpc while the red line shows the density at 6.5 kpc. In both cases, the density is computed for $|z| \leq 2z_d$. Error bars indicate \sqrt{N} uncertainty, where N is the number of particles in each bin.

Because $|\langle V_z \rangle|$ is quite small close to the mid-plane (typically $\sim 5 \text{ km s}^{-1}$), in the right-hand panel of Fig. 6 we show ΔV_z excluding the two bins straddling the mid-plane ($|z| \leq z_d = 250 \text{ pc}$). The velocity asymmetry now stands out even more clearly and reaches values as large as 20 km s^{-1} . The largest expanding velocities are inside the CR radius on the leading edge of the spiral, as can be seen in the annulus $3 \leq R/\text{kpc} \leq 5$. Since the stars overtake the spiral inside CR and are overtaken by it outside CR, the expanding velocities are just ahead of the spiral inside CR and behind it outside this radius. This is most evident by comparing ΔV_z in the two annuli at $3 \leq R/\text{kpc} \leq 5$ and $5 \leq R/\text{kpc} \leq 7$.

The left-hand panels of Fig. 6 show the distributions of V_z in three regions of the disc with large $|\Delta V_z|$. In all three cases, we select particles at some distance above the mid-plane only. Each of the bins has a non-symmetric distribution, with $\langle V_z \rangle$ that is statistically different from zero at more than 3σ . Reflecting these distributions about the $V_z = 0$ axis leads to systematically offset distributions, indicating that the non-zero averages are not due to noise. The two bins at $3.5 \leq R/\text{kpc} \leq 5$ show the vertical kinematics inside CR on the compressing and expanding sides of the spiral. These two bins have the same shape, but the V_z distributions are different. On the expanding side $|\langle V_z \rangle| = 5.4 \pm 0.8 \text{ km s}^{-1}$, while the compressing side has less than half this value of $|\langle V_z \rangle|$. This difference arises because particles leaving the spiral always encounter a more rapidly varying potential than when they enter the spiral.

4 RELEVANCE TO THE MILKY WAY

We have studied the 3D density distribution of strong, grand design spirals using an N -body simulation. At any given radius, the phase of the peak density distribution varies with height, trailing that in the mid-plane with increasing height. At fixed height and radius, the density variation in cylindrical angle ϕ is skewed. Inside CR, the density rises faster

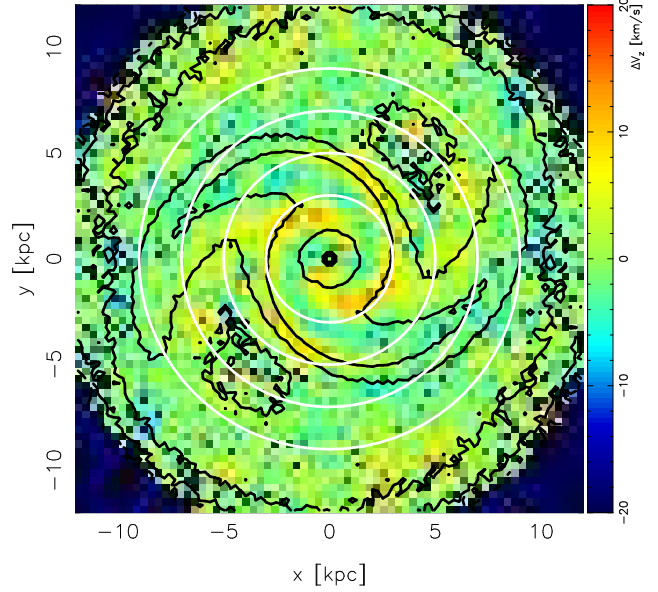


Figure 5. The asymmetry in V_z , ΔV_z , defined in equation (1), for $0 \leq |z| \leq 3z_d$. The white circles range from 3 to 9 kpc in steps of 2 kpc, while the surface density is indicated by the solid black contours.

on the leading side of the spiral than on the trailing. This trend reverses outside CR. These variations with height and angle have not yet been observed in the Milky Way but may be accessible to *Gaia* (Perryman et al. 2001) and the Large Synoptic Survey Telescope (Ivezic et al. 2008). The change in the sense of the skewness across CR, independent of height above the mid-plane, permits measurement of the Milky Way’s spiral pattern speeds purely from the density distribution.

The density variations in spirals lead to $\langle V_z \rangle$ of the order of $\sim 5 - 20 \text{ km s}^{-1}$, increasing with $|z|$. In the stationary frame of the spiral, the motions are compressive as stars enter the spiral arm and expanding as they exit. The expanding motions therefore shift from the leading to the trailing side of the spiral at the CR radius. The recent test particle integrations of Faure et al. (2014) find that spirals induce vertical motions broadly consistent with those found here, including the phase switch across CR. Additionally, in the corotating frame, stars enter the spiral on the shallow density gradient side and exit on the steeper side. As a result, the expansion velocities tend to have larger amplitudes. We also found that $\langle V_z \rangle$ increases with height above the mid-plane, in common with the observations. Although the spiral in our simulation is quite strong and open, we found qualitatively similar behaviour in other simulations.

The vertical motions we found are of similar amplitudes as those observed in the Milky Way. The observed vertical motions have been interpreted as signs of bending waves in the disc, perhaps excited by the Sagittarius dwarf (Gómez et al. 2013). Our highly symmetric disc simulation expressly excludes such bending waves showing that spirals provide an alternative explanation for at least the anti-symmetric part of the observed kinematics. Our simulation shows that these motions are present also when the disc is self-gravitating and the spirals are transient. Weaker, more tightly wound spirals, such as those in the Milky Way,

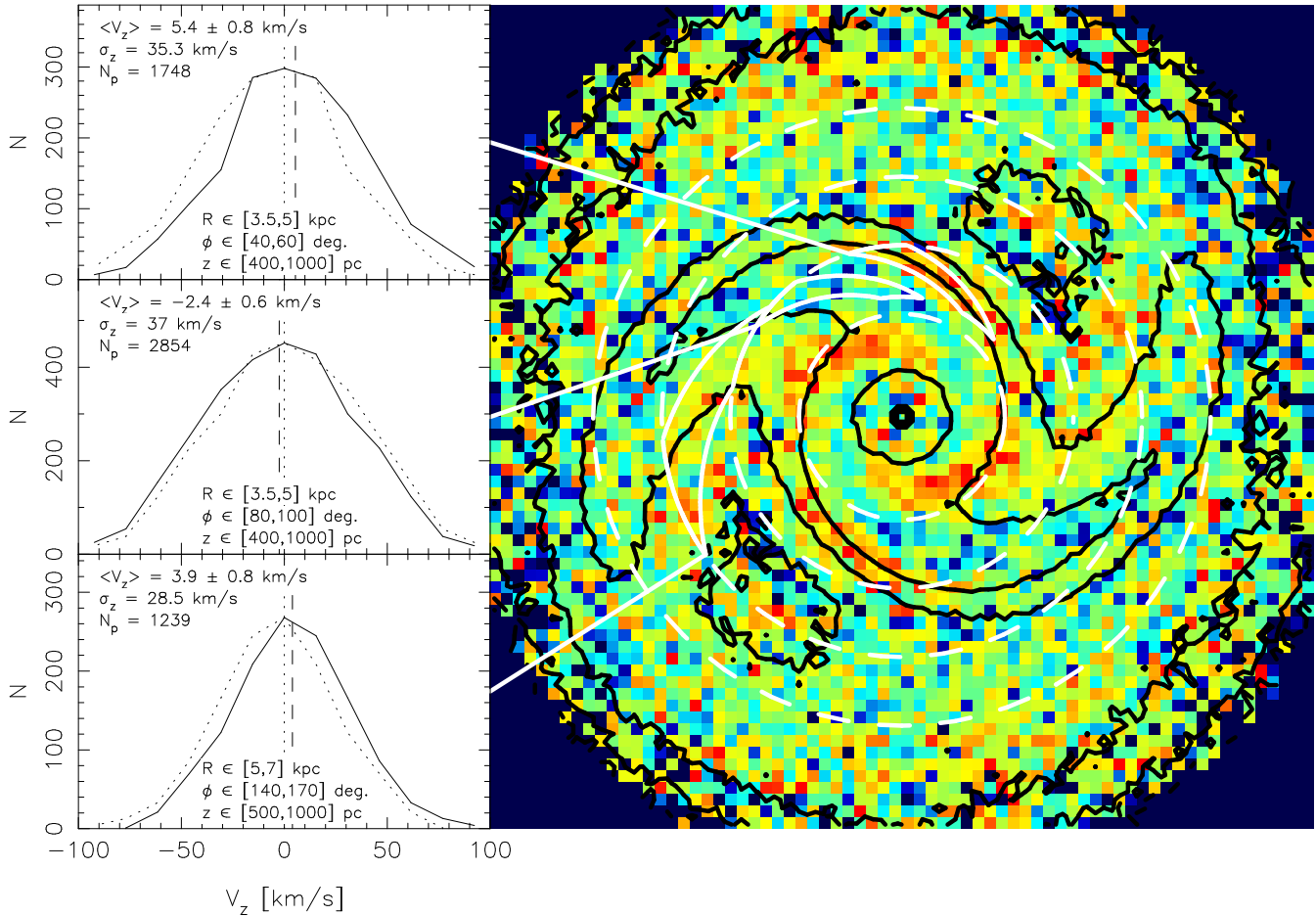


Figure 6. Right: the map of ΔV_z for $z_d \leq |z| \leq 3z_d$, with the same colour scheme as in Fig. 5. The three left-hand panels show the distributions of V_z (solid curves) selected from three regions following a log-spiral curve, and delineated by the solid white lines in the right-hand panel. Each panel lists the number of star particles in each bin, N_p , and the average vertical velocity, $\langle V_z \rangle$ (indicated by the vertical dashed line), together with its uncertainty and the vertical velocity dispersion, σ_z . The vertical dotted line shows $V_z = 0$, while the dotted curve shows the velocity distribution reflected about this line.

may induce smaller motions but the qualitative behaviour should remain similar.

Acknowledgements.

VPD is supported by STFC Consolidated grant no. ST/J001341/1. This project was started during a visit to the Aspen Center for Physics, which is supported by the National Science Foundation under Grant No. PHY-1066293. We thank Rok Roškar and Jerry Sellwood for comments on an earlier draft of the Letter and the anonymous referee for a report that helped improve the clarity of the Letter.

REFERENCES

- Bochanski, J. J., Hawley, S. L., & West, A. A. 2011, *AJ*, 141, 98
- Carlin, J. L., et al. 2013, *ApJ*, 777, L5
- Debattista, V. P., & Sellwood, J. A. 2000, *ApJ*, 543, 704
- D’Onghia, E., Vogelsberger, M., & Hernquist, L. 2013, *ApJ*, 766, 34
- Faure, C., Siebert, A., & Famaey, B. 2014, *MNRAS*, 440, 2564
- Goldreich, P., & Lynden-Bell, D. 1965, *MNRAS*, 130, 125
- Gómez, F. A., Minchev, I., O’Shea, B. W., Beers, T. C., Bullock, J. S., & Purcell, C. W. 2013, *MNRAS*, 429, 159
- Ivezic, Z., et al. 2008, *ArXiv e-prints*
- Julian, W. H., & Toomre, A. 1966, *ApJ*, 146, 810
- Lin, C. C., & Shu, F. H. 1964, *ApJ*, 140, 646
- Meidt, S. E., Rand, R. J., Merrifield, M. R., Debattista, V. P., & Shen, J. 2008, *ApJ*, 676, 899
- Perryman, M. A. C., et al. 2001, *A&A*, 369, 339
- Prendergast, K. H., & Toomre, E. 1970, *AJ*, 75, 674
- Rix, H.-W., & Zaritsky, D. 1995, *ApJ*, 447, 82
- Roškar, R., Debattista, V. P., Stinson, G. S., Quinn, T. R., Kaufmann, T., & Wadsley, J. 2008, *ApJ*, 675, L65
- Schönrich, R. 2012, *MNRAS*, 427, 274
- Schönrich, R., & Binney, J. 2009, *MNRAS*, 396, 203
- Sellwood, J. A. 1983, *Journal of Computational Physics*, 50, 337
- Sellwood, J. A. 2012, *ApJ*, 751, 44
- Sellwood, J. A., & Binney, J. J. 2002, *MNRAS*, 336, 785
- Sellwood, J. A., & Carlberg, R. G. 1984, *ApJ*, 282, 61

- Sellwood, J. A., & Carlberg, R. G. 2014, *ApJ*, 785, 137
Sellwood, J. A., & Kahn, F. D. 1991, *MNRAS*, 250, 278
Sellwood, J. A., & Lin, D. N. C. 1989, *MNRAS*, 240, 991
Sellwood, J. A., & Valluri, M. 1997, *MNRAS*, 287, 124
Siebert, A., et al. 2012, *MNRAS*, 425, 2335
Toomre, A. 1981, in *Structure and Evolution of Normal Galaxies*, ed. S. M., Fall & D. Lynden-Bell (Cambridge: Cambridge University Press), 111
Widrow, L. M., Gardner, S., Yanny, B., Dodelson, S., & Chen, H.-Y. 2012, *ApJ*, 750, L41
Williams, M. E. K., et al. 2013, *MNRAS*, 436, 101
Yanny, B., & Gardner, S. 2013, *ApJ*, 777, 91